npj | clean air

Article

https://doi.org/10.1038/s44407-025-00005-w

Characteristics, emission factors, and health risks of vehicular polycyclic aromatic hydrocarbons

Sohana Debbarma[1], Pradhi Rajeev[2], Tarun Gupta[3] & Harish C. Phuleria[1,4]

This study characterizes vehicular PAHs using roadway tunnel measurements on Mumbai-Pune Expressway, a crucial route in Western India. Dominated by four- to six-ring PAHs (75%-89%), concentrations were influenced by diesel, heavy-duty vehicles (HDVs), and super-emitters. The total PAH emission factor was 52.7(±4.5) μg veh^{-1} km^{-1}. An inverse relationship was observed between PAH molecular weight and volatility of organic carbon (OC). Molecular weight also strongly correlated with mass absorption coefficient (MAC) of brown carbon (BrC), significantly enhancing light absorption. Methanol-soluble BrC exhibited stronger absorption correlation with higher molecular weight PAHs (ΣHMW_{PAH}). Carcinogenic PAHs accounted for 98.9% of total toxicity, with incremental lifetime cancer risk (ILCR) values of ~5 and ~2 per million for adults and children, respectively. These findings highlight the significant contribution of vehicular emissions to urban air quality and health risks, emphasizing the urgent need for mitigation strategies while also providing insights to improve BrC representation in climate models.

Accelerated urbanization and economic growth in India have led to rapid increase in vehicle activity, making vehicular emissions a major source of urban air pollution[1]. Urban-scale simulations suggest that fine particulate ($PM_{2.5}$) pollution originating from vehicle exhaust and on-road resuspended dust, contributes to 25–50%, with hotspots concentrated along major road corridors of Indian cities[2]. Increasing evidence indicates atmospheric pollution, influenced by particle size and chemical composition of carbonaceous aerosols, is associated with climate impacts and significant health risks[3]. A recent study revealed 2.18 million deaths per year are attributable to ambient air pollution in India[4]. Carbonaceous aerosols include organic carbon (OC), such as polycyclic aromatic hydrocarbons (PAHs) along with various other hydrocarbons, elemental carbon (EC), and inorganic carbon compounds, primarily carbonates[5]. Contribution of total carbonaceous aerosol in ambient $PM_{2.5}$ mass measured across different seasons in India is reported to be in the range of ~20–85%[6–8].

Atmospheric PAHs are of particular concern as they are known to have mutagenic and carcinogenic properties[9,10]. These compounds are a group of semi-volatile organics with at least two or more fused carbon and hydrogen aromatic rings, fused together in linear, angular or cluster arrangements[11]. PAHs undergo transformation pathways, leading to the formation of more polar derivatives like nitro- oxy-, and hydroxy PAHs, which can be even more toxic and mutagenic than their parent PAHs[12]. Depending on their molecular weight, PAHs exist in different physical states: 2- and 3-ringed PAHs are typically found in the gaseous phase, while PAHs with more than 5 rings tend to associate with particulate matter, 4 ringed-PAHs can exist in both gaseous and particulate phases[13]. Higher molecular weight and enhanced polarity leads to increase in the toxicity of PAHs[14]. Based on their toxicity and abundance, the United States Environmental Protection Agency (USEPA) has identified sixteen priority PAHs[11]. Primarily, the effect of PAHs on human health is based on the duration and route of exposure (through inhalation, ingestion, and dermal contact), concentration of PAHs to which one is exposed to, and the relative toxicity of PAHs[10].

Growing evidence from several studies has indicated that PAHs can influence the optical properties and radiative effects of brown carbon (BrC), which is the light-absorbing component of OC[15,16]. BrC absorbs light in the ultraviolet-to-visible spectrum, with its absorption exhibiting a strong dependence on wavelength[17]. PAHs have been identified as important BrC chromophores due to their large conjugated polycyclic structures, which impart strong light-absorbing properties in the near-UV range (300–400 nm)[18,19]. Many studies[20–22] have shown that water-soluble organic carbon (WSOC) fractions, especially humic-like substances (HULIS) and other individual WSOC species, contribute to the light absorption of organic aerosols. However, while the water-soluble fraction of BrC has been extensively studied[23–25], the contribution of water-insoluble species like

[1]Centre for Climate Studies, Indian Institute of Technology Bombay, Mumbai, 400076, India. [2]Department of Civil and Environmental Engineering, Indian Institute of Technology Patna, Patna, 801106, India. [3]Department of Civil Engineering, Indian Institute of Technology Kanpur, Kanpur, 208016, India. [4]Environmental Science and Engineering Department, Indian Institute of Technology Bombay, Mumbai, 400076, India. e-mail: phuleria@iitb.ac.in

PAHs to light absorption properties of atmospheric pollutants remains largely unquantified, in particular, from vehicular emissions.

PAHs from on-road vehicles originate from exhaust as well as non-exhaust sources such as brake wear, tyre wear, asphalt, and resuspended dust[26,27]. The characteristics and emission factors of PAHs emitted from vehicles are significantly influenced by factors such as engine type, operating conditions, fuel composition, vehicle mileage, and the presence of catalytic converters[28]. Sampling in roadway tunnels provide a more realistic traffic profile than laboratory-based dynamometer tests[29], as they allow to investigate the characteristics of pollutants discharged from heterogenous mix of vehicle (or fleet composition) operated at controlled conditions like fixed vehicle speed and least influence of meteorological parameters inside the tunnel. Many recent studies in India have reported that on-road exhaust emission is a significant source of PAHs in urban areas[14,30–33]. However, so far no attempt has been made to characterize, and estimate emission factors of PAHs from real-world vehicular fleet. To the best of our knowledge, this is the first study, to report the profile and emission factors of real-world vehicular fleet PAHs using road tunnel measurement in India.

In this study, the primary objectives were to: (1) characterize on-road vehicular PAHs and assess the influence of traffic parameters on PAHs, (2) investigate the association of PAHs with bulk chemical composition and light absorption properties of BrC, (3) assess the leading health risks, and (4) estimate vehicular PAHs emission factors.

Results and Discussion

Traffic flow characteristics

The hourly average traffic of 1560(±410) vehicles consisted 80% LDVs and 20% HDVs, driving at an average speed of 78(±4) km h^{-1}. Peak traffic observed during morning rush hours was 21% higher than afternoon non-rush hours. There was no significant difference ($p > 0.05$) in traffic volume and composition between North-and South-Bore of the Kamshet-I Tunnel (KT). Higher HDV fraction was observed during the early morning hours which was due to the movement restriction of HDVs in Mumbai (restriction time: 8:00 am–11:00 am and 5:00 pm–9:00 pm) and in Pune (between 7:00 am and 9:00 pm). The weekend traffic was observed to be 27% higher than the weekday traffic indicating inter-city traffic movement. Diesel vehicles across all vehicle class dominated the fleet (51%) followed by gasoline vehicles (41%), and compressed natural gas (CNG) vehicles comprised 8% of the fleet. While the share of gasoline vehicles was higher during the morning hours, the share of diesel vehicles were observed to higher during the afternoon hours. A significant share (14%) of older vehicles (>10 years: pre-2009 vehicles) was observed in the fleet. Across all vehicle class, aged vehicles were observed to be highest in trucks (23%), followed by light commercial goods vehicles (LCGVs) and buses (22%) and cars (11%). In terms of emission standards, vehicles that comply with poorer and obsolete emission technologies: Bharat Stage (BS) III, II, and I were observed to be most prevalent among trucks (44%), followed by buses (40%), LCGVs (37%), and cars (18%). Super-emitters (SE), characterized as older, poorly maintained, and overloaded heavy-duty diesel vehicles, accounted for 21% (±3%) of the total fleet[34].

PAHs levels and composition

The average (±standard deviation) mass concentration of all sixteen PAHs at the entry and exit of the tunnel are shown below in Fig. 1. Concentration of all PAHs at the tunnel exit were significantly higher (1.4 to 3.8 times) than at entry of the tunnel ($p < 0.05$). The average concentrations of all sixteen PAH compounds (ΣPAH_{16}) at the tunnel entry and tunnel exit were 107(± 46) and 203(± 72) ng m^{-3}, respectively. The molecular weights of 2–3 rings PAHs are 128 to 178 g mol^{-1}, 4 rings: 202 to 228 g mol^{-1} and 5–6 rings: 252 to 276 g mol^{-1}. The PAHs were classified into (1) low-molecular weight PAHs (ΣLMW_{PAHs}) which include compounds of 2 and 3-rings (i.e. NAP, ACY, ACE, FLU, PHE, and ANT), and (2) high-molecular weight PAHs (ΣHMW_{PAHs}) which include 4–6 rings compounds (i.e. FLA, PYR, BaA, CHR, BbjF, BkF, BaP, DahA, IcdP, and BghiP. The percentage mass fraction of each individual PAH to the total PAH concentration at tunnel entry and tunnel exit has been provided in Supplementary Fig. 1.

ΣHMW_{PAHs} concentrations were significantly ($p < 0.05$) higher than ΣLMW_{PAHs} at both the tunnel entry and tunnel exit. The ΣHMW_{PAHs} accounted for 75% to 89% of the total PAHs concentrations and they were significantly higher during the morning hours when the traffic volume was higher. These findings were similar to previous road tunnel study[13] that reported high molecular weight PAHs collectively accounted for about 88% of the total PAHs at the tunnel entry and exit. Also, as Zhao et al.[35] reported that most of the PAHs emissions from traffic sources were high-rings PAHs, it can be implied that the PAHs emissions were driven by vehicles at the tunnel, especially at the exit. Among the high molecular weight PAHs too, it was observed that the 4-rings PAHs were higher than the 5-6 rings PAHs, this can be due to higher fraction of diesel vehicles in the study tunnel. The 4-ring PAHs constituted the highest proportion of 46(±8)% of the total PAH concentration. Previous road tunnel study in China too reported the highest contribution of 4-ring PAHs to be around 58%[36]. The 4-rings PAHs mainly derive from diesel vehicle emissions, while 5–6 rings PAHs were reported to be linked with gasoline vehicle emissions[37]. While the exit/entry ratio in HMW_{PAHs} were upto 3 times higher as compared to the exit/entry ratio in LMW_{PAHs} this too indicated the levels at the tunnel exit were true signature of vehicular exhausts and the tunnel entry levels were influenced by other ambient sources. Rajeev et al. [38] highlighted HMW_{PAHs} as molecular precursor for soot particles. The presence of high fraction of diesel vehicles in both LDVs and HDVs led to the high contribution of HMW_{PAHs} to total PAHs at the study tunnel.

Diagnostic ratios used for distinguishing traffic and non-traffic emissions, diesel and gasoline-related emissions, calculated from the concentration differences obtained in this study are listed and compared with previous studies[35,39–41] in Supplementary Table 1. These ratios also show the

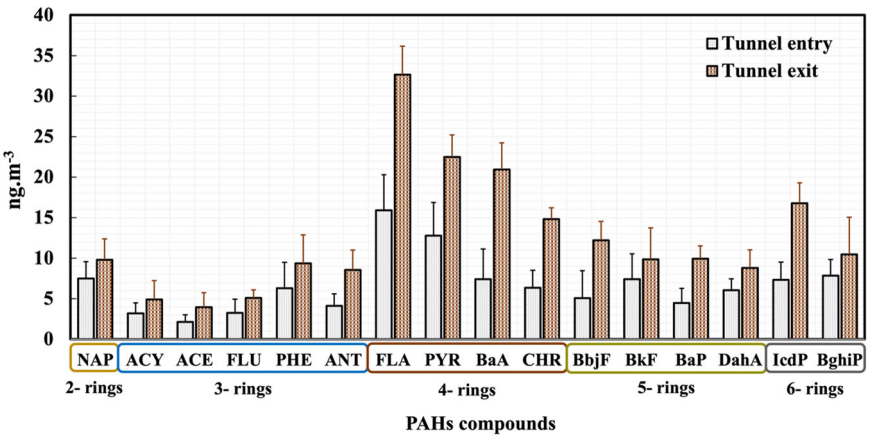

Fig. 1 | Average PAHs concentration in ng m^{-3} at the entry and exit of Kamshet-I tunnel. [Note: Number of samples, $N = 14$ (Tunnel entry), $N = 14$ (Tunnel exit)].

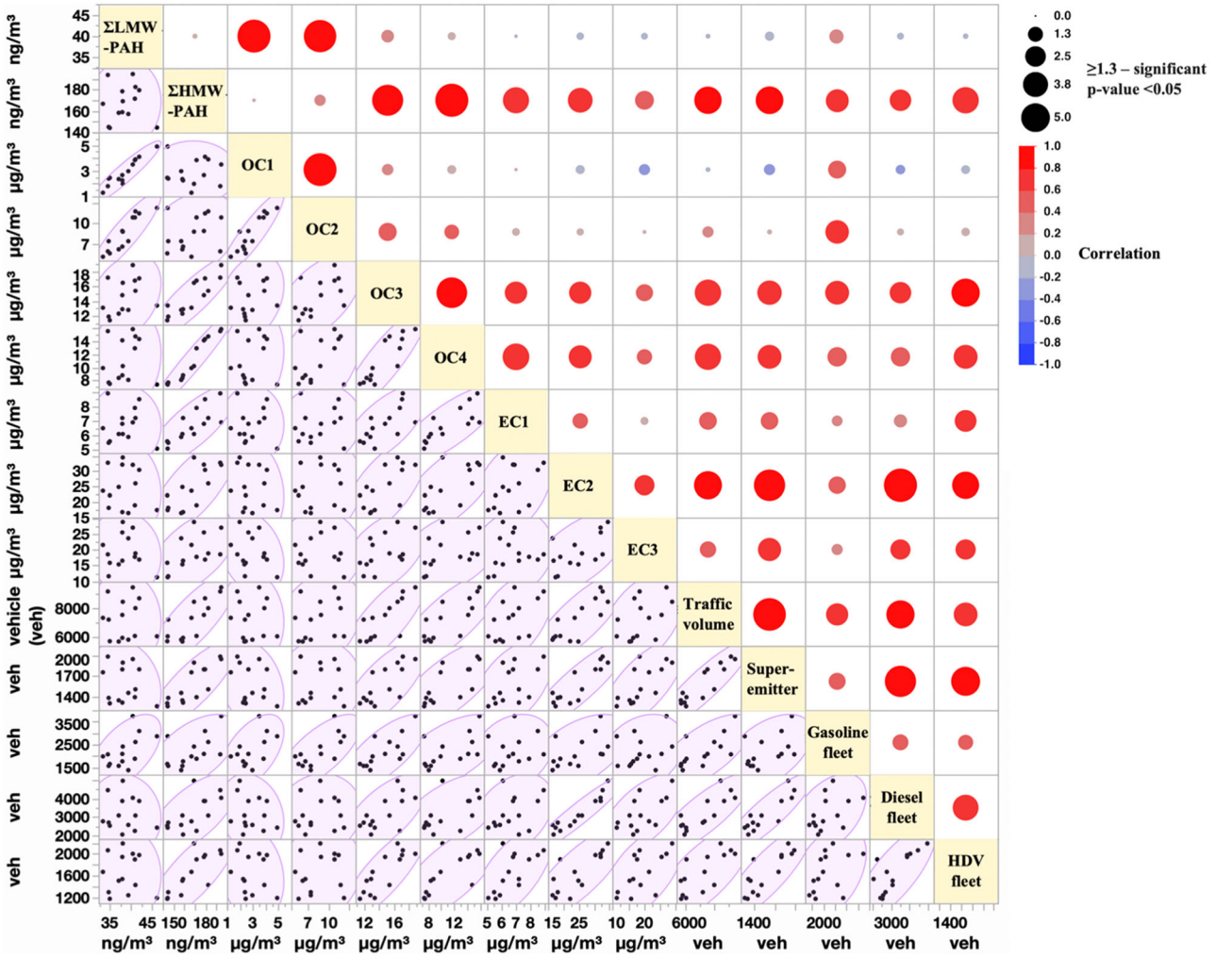

Fig. 2 | Scatter matrix plot of Pearson correlation of PAHs concentrations, carbonaceous fractions and traffic parameters. All the pollutant concentrations here are of at the tunnel exit (Number of samples, $N = 14$). [Note: Correlations between the parameters are denoted by the coloured circles in the figure, red: positive correlation and blue: negative. Association between the parameters is represented by the size of the circles, bigger the circles show stronger the association, and smaller circles show weaker association].

intra-source variability and inter-source similarities. BaP/BghiP ratio of 0.57(±0.03) at the tunnel entry suggested the contribution of non-traffic sources and influence of other ambient sources including biomass burning from the neighbouring village and photochemical activities. While at the tunnel exit higher BaP/BghiP ratio of 0.84(±0.14) indicated significant contribution of traffic sources. $\Sigma LMW_{PAH}/\Sigma HMW_{PAH}$ ratio <1 and ΣCOMB/ΣPAHs ratio close to 1 indicated pyrogenic sources and combustion signature, respectively at both tunnel entry and tunnel exit. The IcdP/(IcdP+BghiP) ratio of 0.48(±0.07) and 0.63(±0.11) at tunnel entry and tunnel exit, respectively, indicated the contribution of diesel exhaust emissions. Overall, ratios of FLA/(FLA + PYR), BaA/(BaA+CHR), and IcdP/(IcdP+BghiP) revealed higher diesel exhaust signature which can be attributed to the higher fraction of diesel vehicles and HDVs in the fleet.

Association of PAHs with bulk chemical species and traffic parameters

Scatter matrix plot of Pearson correlation at 95% confidence interval (CI) were developed to examine the association between the concentrations of the PAHs compounds, carbonaceous fractions and traffic parameters as shown in Fig. 2. Collectively, all the higher molecular weight (ΣHMW_{PAH}) significantly ($p < 0.05$) correlated with all traffic parameters, indicating that the HMW_{PAHs} were predominantly influenced by the vehicles driving inside the tunnel. ΣHMW_{PAH} was strongly influenced by the traffic volume ($R = 0.88$), super-emitters ($R = 0.84$) and HDVs ($R = 0.77$). Diesel and gasoline vehicles also significantly ($p < 0.05$) influenced the ΣHMW_{PAH} concentrations. Similar findings were reported by previous roadway tunnel studies that have reported >3-rings PAHs from vehicular sources[13,42–45]. Even in Indian cities of Allahabad and Kanpur, the higher percentage contribution of ΣHMW_{PAH} to the total PAHs, mainly the 4-ring PAHs (FLA, PYR, BaA, CHR) was contributed to diesel exhaust emissions[14]. The ΣLMW_{PAH} concentrations did not show any significant ($p > 0.05$) association with any of the traffic parameters, indicating they were driven by other petrogenic sources.

The bulk chemical composition: OC and EC profiles have been presented in our previous study[46]. While the ΣLMW_{PAH} showed strong association with OC1 and OC2 ($R > 0.91$), ΣHMW_{PAH} showed strong association with OC3, OC4, EC1 and EC2 ($R > 0.75$). The associations between the molecular weights of the PAHs and the volatility of OC fractions were examined and are presented in Supplementary Fig. 2. An inverse relationship between molecular weight and volatility was established. A strong and significant ($p < 0.05$) association between ΣHMW_{PAH} and low volatile OC (LVOC) ($R = 0.96$) revealed that high molecular weight PAHs are less volatile. Conversely, the association between ΣLMW_{PAH} and high volatile OC (HVOC) ($R = 0.92$) indicated that lower molecular weight

PAHs exhibit higher volatility. Weak association was observed between HVOC and ΣHMW_{PAH} ($R = 0.18$), as well as between LVOC and ΣLMW_{PAH} ($R = 0.2$). This also indicate the difference in sources that originate HVOC and $\Sigma HMW_{PAH.}$ Vehicular exhausts, particularly diesel vehicles release more LVOC at higher temperature than HVOC[46], and they emit more of HMW_{PAH}[13]. Diesel vehicles and HDVs led to higher concentration levels of LVOC than HVOC from the measured fleet. Consequently, the higher abundance of LVOCs resulted in the increased levels of HMW_{PAH} relative to LMW_{PAH}. This relationship underscores the significant role of diesel emissions in shaping the chemical profile of atmospheric organic pollutants particularly in urban environments where diesel-powered vehicles are prevalent.

Correlation of PAHs with light absorption properties of BrC

Light absorption properties of the measured aerosols have been presented in our previous study[46]. The correlations between PAHs and other light absorption properties like the mass absorption coefficient (MAC) and absorption Ångström exponent (AAE) of BrC were examined (shown in Supplementary Fig. 3 and Supplementary Fig. 4, respectively). A strong correlation ($R = 0.93$) was observed between low volatile ΣHMW_{PAH} and $MAC_{MS\text{-}BrC}$ at 370 nm, indicating that with increasing molecular weight, the light absorbing property may increase. It also suggests ΣHMW_{PAH} are associated with other compounds (LVOCs) emitted from the same source, that are light absorbing. Strong association between LVOC and $MAC_{MS\text{-}BrC}$ ($R = 0.87$) was observed, as shown in Supplementary Fig. 5. This highlighted the contribution of hydrophobic OC fraction, which is dominated by HMW_{PAH}, to the light-absorbing properties of BrC. Also reported by a previous study that PAHs are likely contributors to BrC chromophores, originating from common sources, including vehicular exhaust[47]. The high volatile ΣLMW_{PAH} showed weak correlation with both water-soluble mass absorption coefficient ($MAC_{ws\text{-}BrC}$) as well as methanol-soluble MAC ($MAC_{MS\text{-}BrC}$) at 370 nm. Similar findings were reported by Saleh et al. [48] where inverse correlation of BrC light absorption with volatility and direct correlation of light absorption with molecular weight was observed. Strong correlation between ΣHMW_{PAH} and $MAC_{MS\text{-}BrC}$ potentially may be due to methanol's extraction efficiency of around 85%[49].

Methanol extracts a broader spectrum of organic compounds, including both hydrophilic and hydrophobic compounds, unlike water, which extracts only hydrophilic compounds. These hydrophobic compounds include higher molecular weight PAHs, mostly derived from fossil fuel combustion[50]. Saleh et al.[48] highlighted that with decreasing solubility in water as well as in organic solvents like methanol, the light absorbing property of the hydrophobic compounds increases. MS-BrC had higher absorption than WS-BrC across all wavelengths between 300 and 800 nm, which is consistent with the previous studies as well[50,51]. The wavelength dependence of light absorption, indicated by absorption Ångström exponent (AAE), between 370 and 550 nm for both water- and methanol-extracts was investigated. We observed strong correlation between LMW_{PAHs} and $AAE_{MS\text{-}BrC}$ ($R = 0.91$), while no correlation ($R = 0.05$) between LMW_{PAHs} and $MAC_{MS\text{-}BrC}$ was observed, which indicates LMW_{PAHs} has higher AAE, and lower MAC compared to HMW_{PAHs}. This corroborates well with the BrC-BC light absorption continuum, where MAC is inversely linked with AAE as reported by Navinya et al. [52], and directly proportional with the molecular weight[48]. These findings can be used to represent the BrC absorption variability from real-world vehicular emissions in climate models. While in this study, light-absorbing HMW_{PAHs} and their relationship with the bulk species and the light absorption properties were studied, nitro-PAHs that are also known to be highly light absorbing[53] have not been included, which is a limitation of the study.

Health risk characterization

Based on the concentrations of each PAH compound and their corresponding toxic equivalent factor (TEF) values, benzo[a]pyrene-equivalent (BaP_{eq}) concentrations,the cancer risks were estimated. The average $\sum BaP_{eq}$ concentration was 13.5(±5.6) ng m^{-3} and 25.2(±4.9) ng m^{-3} at the tunnel entry and tunnel exit, respectively, these values exceed the standard. The current regulatory limit for BaP in India is established by the National Ambient Air Quality Standards (NAAQS) at a daily average concentration of 1 ng m^{-3}. Table 1 presents the values of BaP_{eq}, lifetime average daily dose (LADD), and incremental lifetime cancer risk (ILCR) measured at the tunnel entry. The values at tunnel exit have been presented in Supplementary Table 2. Although previous tunnel studies[36] have reported ILCR values at both tunnel exit and tunnel entry, the ILCR values at the tunnel exit represent extreme exposure scenarios. Since the probability of continuous exposure inside a tunnel environment is low, these values are less relevant for general population risk assessment. While ILCR values at the tunnel entry reflect the risk for populations with high exposure, such as roadside residents, inter-city travellers, and freight vehicle drivers within the study area. These values provide insight into the potential health risks from vehicular emissions in high-exposure environments, such as near roadways or inter-city expressways. BaP_{eq} concentration for the seven carcinogenic PAHs (BaA, CHR, BbjF, BkF, BaP, DahA, and IcdP) identified by WHO International Agency for Research on Cancer (IARC) accounted for 98.9% of the total PAHs.

The USEPA uses ILCR to evaluate cancer risks from long-term carcinogen exposure, ILCR below 10^{-6} is acceptable, 10^{-6} to 10^{-4} indicates moderate risk, and above 10^{-4} signals high risk[54]. The ILCR values follow BaP>DahA>IcdP>BbjF for both adult and children at the tunnel exit, while at the tunnel entry it was DahA>BaP>BkF>IcdP for both adult and children at the tunnel entry. In this study, the observed ILCR values of 8.9 in one million and 3.7 in one million for adult and children, respectively at the tunnel exit are approximately double the ILCR values observed for both adult and children at the tunnel entry. This increase highlights the significant health risks associated with exposure to elevated levels of vehicular emissions. These values are similar to the ones reported in ambient $PM_{2.5}$ over central Indo-Gangetic Pain with significant contribution of vehicular sources: 4.5 to 8.1 in a million for adult and 2.6 to 4.8 in a million for children[14]. However, the ILCR values from this study are notably higher than those reported for vehicular emission exposure at a national highway (NH) site ($1.8E^{-10}$ for adult, $5E^{-11}$ for children) and a busy traffic site ($1.7E^{-10}$ for adult, $4.8E^{-11}$ for children) in Asansol city, India[32]. Additionally, another road tunnel study in Turkey reported estimated cancer risks of urban population due to inhalation of PAH: 1.1 to 4.9 in one million[55]. While the observed ILCR values in this study fall under moderate risk, their magnitude highlights the pressing need for implementing effective mitigation measures, such as stricter vehicular emission standards (especially for diesel vehicles and HDVs), and a transition to cleaner energy vehicles, which collectively would help minimize pollutant exposure and associated health risks.

Estimated emission factor (EF) of PAHs

PAHs EFs (in μg veh^{-1} km^{-1}) were estimated using the distance based approach, and they are presented in Fig. 3. The total average $PM_{2.5}$-bound PAH (ΣPAH_{16}) EF in this study was 52.7(± 4.5) μg veh^{-1} km^{-1}. ΣHMW_{PAH} EF of 42.1(±8.6) μg veh^{-1} km^{-1} contributed to ~80% of the total EF. Similar EFs were reported by previous tunnel studies with HDV fleet: 50.3 μg veh^{-1} km^{-1} by Alves et al.[56] in Liberdade Avenue tunnel, Portugal, and 61 μg veh^{-1} km^{-1} by Zhao et al.[35] in Yangkou Tunnel, China. However, the EFs of 4-5 rings PAHs that are driven by diesel vehicles and HDVs were lower in this study as compared to the ones reported by other studies with HDV fleet, this could be because there were only 20% HDV in our study tunnel whereas, the tunnel in Portugal had all HDV fleet and the tunnel in China had all HDV fleet. The EF from this study was about 2 times higher than the EFs reported from LDV and gasoline dominated tunnels[13,57]. This could be because of the presence of HDVs, super-emitters and higher diesel vehicles in the fleet as compared to the all LDV or gasoline dominated fleet. Chen et al.[43] reported that the PAHs EF from diesel vehicles are 3.37 times higher compared with that from gasoline vehicles. Ho et al.[42] observed that diesel vehicles emitted 5.45 times PAHs compared to gasoline vehicles.

Table 1 | Lifetime average daily dose (LADD) and Incremental lifetime cancer risk (ILCR) from $PM_{2.5}$-bound 16 priority PAHs to humans through inhalation measured at the entry of Kamshet-I tunnel

PAHs	BaP_{eq} (ng m^{-3})	LADD (mg kg^{-1} day^{-1})		ILCR (10^{-6})	
		Adult	Children	Adult	Children
NAP	0.007	8.5E−10	3.6E−10	2.7E−03	1.1E−03
ACY	0.003	3.6E−10	1.5E−10	1.1E−03	4.7E−04
ACE	0.002	2.4E−10	1.0E−10	7.5E−04	3.1E−04
FLU	0.003	3.7E−10	1.5E−10	1.2E−03	4.8E−04
PHE	0.006	7.2E−10	3.0E−10	2.2E−03	9.3E−04
ANT	0.041	4.7E−09	2.0E−09	1.5E−02	6.1E−03
FLA	0.016	1.8E−09	7.6E−10	5.6E−03	2.3E−03
PYR	0.013	1.5E−09	6.1E−10	4.5E−03	1.9E−03
BaA	0.742	8.5E−08	3.5E−08	2.6E−01	1.1E−01
CHR	0.064	7.3E−09	3.0E−09	2.3E−02	9.4E−03
BbjF	0.506	5.8E−08	2.4E−08	1.8E−01	7.5E−02
BkF	0.742	8.5E−08	3.5E−08	2.7E−01	1.1E−01
BaP	4.5	5.1E−07	2.1E−07	1.6×10^0	6.6E−01
DahA	6.1	6.9E−07	2.9E−07	2.1×10^0	8.9E−01
IcdP	0.732	8.4E−08	3.5E−08	2.6E−01	1.1E−01
BghiP	0.078	9.0E−09	3.7E−09	2.8E−02	1.2E−02
∑16PAHs	13.5	1.54E−06	6.42E−07	4.8×10^0	2.1×10^0
$\sum 7PAHs_{carcinogen}$	13.3	1.52E−06	6.34E−07	4.7×10^0	2.0×10^0
$\sum LMW_{PAH}$	0.063	7.2E−09	3.0E−09	2.3E−02	9.4E−03
$\sum HMW_{PAH}$	13.42	1.53E−06	6.39E−07	4.76×10^0	1.97×10^0

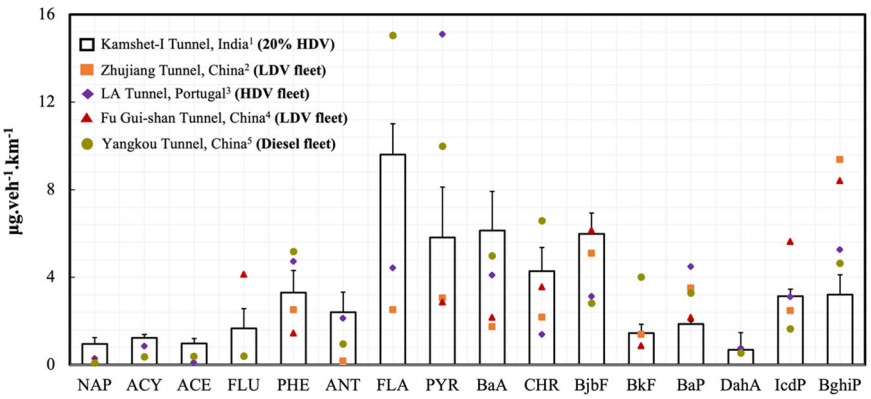

Fig. 3 | Estimated PAHs emission factors and comparison with other previous tunnel studies. [1]This study; [2]He et al.[57]; [3]Alves et al.[56]; [4]Fang et al.[13]; [5]Zhao et al.[35].

Methods

Roadway tunnel sampling

The field campaign was conducted in the Kamshet-I roadway tunnel (18°44′15″N, 73°31′56″E), located on one of India's busiest inter-city arterial corridors in terms of both passenger and goods movements, Mumbai-Pune Expressway in December 2019. The tunnel has two unidirectional bores, the North Bore (NB): Mumbai to Pune (949 m in length) and the South Bore (SB): Pune to Mumbai (969 m in length), the detailed description of the tunnel is given in our previous study[34]. The ventilation system inside the tunnel consisting of jet fans were all closed during the sampling period so as to ensure that the accumulation ensure the measured aerosols inside the tunnel were solely attributed to emissions from the vehicles traversed.

Filter-based aerosol measurements were carried out concurrently at the entry and exit of the tunnel for consecutive two weeks (NB: 6th to 12th December, 2019 and SB: 13th to 19th December, 2019). $PM_{2.5}$ gravimetric samples were obtained using MiniVol samplers (Airmetrics, USA[35] operated at an airflow rate of 5 L min^{-1}, along with a multi-stream PM sampler[58] with an airflow of ~20 L min^{-1}. The tunnel entry samples provided an ambient background concentration which was subtracted from the exit concentrations to calculate the elevated vehicle-induced concentration. The sampling stations were located 50 m away from the entrance and about ~100 m away from the exit of the tunnel, and the instruments were set up on the sidewalks at a height of 1.5 m above the road surface. Gravimetric samples were collected over five-hour intervals during two distinct periods: the morning peak traffic hours (7:00 AM to 11:59 AM) and the afternoon non-peak traffic hours (12:00 PM to 5:00 PM). These sampling periods were determined based on preliminary trial measurements conducted beforehand to assess the prevailing traffic conditions.

A high-resolution video camera was used to examine the traffic fleet based on its volume and composition every hour during the measurement period. From the recorded videos, the vehicles were counted manually and were classified into: (1) light-duty vehicles (LDV): passenger cars and light

commercial goods vehicles (LCGVs) that weigh ≤3.5 tonnes, (2) heavy-duty vehicles (HDV): buses and trucks that weigh >3.5 tonnes. Around 2100 license plate numbers were manually collected randomly from all the vehicle categories. Two-wheelers and three-wheelers were not allowed to ply inside the tunnel due to restrictive movements on the high-speed expressway. Individual vehicle information like vehicle makes and model, fuel type, age of the vehicle, and emission standard were obtained from the license plate numbers using a mobile application-based software, "RTO vehicle information"[34,59]. The spot speed of the vehicles was captured using a velocity speed gun (Bushnell, USA[60]). The wind speed inside the tunnel was measured using a hot-wire anemometer (model GM8903, BENETECH, China) and was positioned inside the tunnel to capture representative airflow conditions. Due to the confined boundary conditions of the tunnel, the movement of vehicles created a piston effect, driving the wind in the same direction as the vehicles. The wind speed recorded by the anemometer corresponds to the airflow predominantly parallel to the tunnel axis. This measurement captures the vector component of wind speed aligned with the tunnel, which is the primary airflow direction influenced by vehicle movement.

Chemical analysis

Carbonaceous content (OC and EC) in the measured $PM_{2.5}$ samples were analysed using the Desert Research Institute (DRI) Model 2015 thermal and optical carbon analyzer. Under the Interagency Monitoring of Protected Visual Environments (IMPROVE_A) Protocol, eight fractions of carbon were derived in two phases of heating: OC1, OC2, OC3, and OC4 (volatile) evolved in a non-oxidizing Helium (He) atmosphere; residual OC (OP), a pyrolyzed carbon fraction and EC1, EC2, and EC3 (non-volatile) evolved in a 2% O_2 and 98% He atmosphere[61,62]. In this study, OC fractions were categorized into two groups: (1) high volatile organic carbon (HVOC), referred to as the sum of OC1 and OC2, emitted at 180 °C and 280 °C, respectively, and (2) low volatile organic carbon (LVOC), referred to as the sum of OC3 and OC4, emitted at 480 °C and 580 °C, respectively. The light absorption properties of BrC were analysed using the Ultraviolet-Visible spectrophotometer (UV-VIS Evolution 220, Thermo-Fisher) in water and methanol extracts. The light absorption spectra of the extracted samples were measured from 300 to 800 nm. Light absorption properties such as mass absorption coefficient (MAC) at 370 nm and the spectral dependence of absorption or absorption Ångström exponent (AAE) between 370 and 550 nm of water-soluble brown carbon (WS-BrC) and methanol soluble brown carbon (MS-BrC) were estimated using empirical Eqs. (1) and (2), respectively. A detailed explanation of the methods is provided in our previous study[46].

$$\mathrm{MAC}_{\lambda}\left(\mathrm{m}^2\mathrm{g}^{-1}\right) = \frac{\mathrm{b}_{\mathrm{abs}}}{\mathrm{C}} \tag{1}$$

$$\mathrm{AAE}_{\lambda_{1-\lambda_2}} = -\frac{\ln(\mathrm{b}_{\mathrm{abs}}(\lambda_1)/\mathrm{b}_{\mathrm{abs}}(\lambda_2))}{\ln(\lambda_1/\lambda_2)} \tag{2}$$

where b_{abs} is the absorption coefficient at $\lambda = 370$ nm, C represents the measured mass concentration of WSOC (C) for water soluble and OC (C) for methanol soluble extract. λ_1 and λ_2 used for AAE calculation are 370 and 550 nm, respectively.

PAHs analysis was carried out on the remaining $PM_{2.5}$ samples collected on quartz fibre filters after OC-EC analysis. In this study, the sixteen priority USEPA PAHs, which include 2-ringed PAH: Naphthalene (NAP); 3-ringed PAH: Acenaphthylene (ACY), Acenaphthene (ACE), Fluorene (FLU), Phenanthrene (PHE), Anthracene (ANT); 4-ringed PAH: Fluoranthene (FLA), Pyrene (PYR), Benzo[a] Anthracene (BaA), Chrysene (CHR); 5-ringed PAH: Benzo[b,j] Fluoranthene (BbjF), Benzo[k] Fluoranthene (BkF), Benzo[a] Pyrene (BaP), Dibenzo[a,h] Anthracene (DahA); 6-ringed PAH: Benzo[g,h,i] Perylene (BghiP), and Indeno[1,2,3-c,d] Pyrene (IP) were analysed. Our study focussed on particle-phase PAHs only and gas-particle phase partitioning was not investigated. As lower molecular weight PAHs (in particular those < 4-rings) can have substantial gas-particle phase partitioning, our results are a conservative estimate of the PAHs profiles and emission factors. Gas chromatography coupled with mass spectrometry (GC-MS) was used to separate, identify and quantify the target PAHs by solvent extraction method. For sample extraction and preparation, the solvents dichloromethane (DCM), acetone and toluene of HPLC grade (purity ≥99.8%; Merck) were used for sample extraction and preparation (detailed explanation given in Rajeev et al.[14]. Quantification of all target compounds was done on GC-MS (Agilent GC: 7890B; MSD: 5977B) equipped with a capillary column (DB-5MS column) and helium was used as a carrier gas[14].

Quality control and quality assurance (QA/QC)

Mini volume (MiniVol) samplers and multi-stream PM sampler underwent routine flow rate calibration to ensure precise sampling. Quality control measures were meticulously implemented to ensure the reliability and accuracy of the data, including the preparation and analysis of both laboratory and field blank samples ($N = 2$ for each time period, at the tunnel entry and tunnel exit). Some contamination was observed in laboratory blanks, with higher than 25% of mean tunnel sample concentrations were excluded. The analytical field blank values for each target compound were significantly lower than the concentrations detected in the actual samples, validating that contamination during the process was minimal. The concentrations of all the PAH compounds reported in this study are field blank corrected mass concentration. Additionally, as a quality control measure, the variability in internal standards (phenanthrene d-10 and perylene d-12 of 150 ng each was spiked to standards and samples) response across the analysed samples was found to be small (within ±5%) between subsequent runs which ensured the consistency and accuracy of the analytical procedure.

Human health risk assessment

Inhalation of $PM_{2.5}$ bounded PAHs was regarded as risk on human health estimated in this study. Benzo[a]pyrene (BaP) is recognized as one of the most potent carcinogens among PAHs[63]. The potential health risks associated with PAH exposure through inhalation pathway were assessed using the BaP equivalent concentration (BaP_{eq}) and incremental lifetime cancer risk (ILCR) methodologies recommended by the US Environmental Protection Agency (EPA)[54].

Carcinogenic risk

To evaluate the cumulative carcinogenic risk associated with different PAHs, a toxicity equivalent factor (TEF) is assigned to each PAH compound relative to BaP, which can be used as the reference compound for health risk assessment[64]. It allows each PAH's concentration to be adjusted based on its carcinogenic potency compared to BaP[32]. BaP_{eq} of individual PAHs and total carcinogenic equivalent concentration was calculated using Eq. (3).

$$\mathrm{TBaP}_{\mathrm{eq}} = \sum_{\mathrm{i}=1}^{\mathrm{n}} (\mathrm{C}_{\mathrm{i}}\,\mathrm{x}\,\mathrm{TEF}_{\mathrm{i}}) \tag{3}$$

where, $TBaP_{eq}$ represents the total carcinogenic BaP equivalent concentration (in ng m^{-3}); C_i represents the concentration of individual PAH compound and TEF_i represents corresponding toxicity equivalent factor of the PAHs. The TEF values of NAP, ACY, ACE, FLU, PHE, FLA, and PYR are 0.001; ANT, CHR, and BghiP are 0.01; BaA, BbjF, BkF, and IcdP are 0.1; BaP and DahA are 1.

Incremental lifetime cancer risk

The increased risk of cancer over a lifetime as a result of continuous exposure to a carcinogen is represented by incremental lifetime cancer risk (ILCR). ILCR due to PAHs from respiratory exposure was calculated using lifetime average daily dose (LADD) and cancer slope factor (CSF). LADD refers to the intake amount (mg) of a chemical species per unit of body weight (kg) over an extended period, typically accounting for chronic or

lifetime exposure[14], used to evaluate the potential health impacts of long-term exposure to hazardous environmental species. Equations (4) and (5) are used to calculate LADD and ILCR, respectively.

$$\mathrm{ILCR} = \mathrm{LADD\ x\ CSF} \tag{4}$$

$$\mathrm{LADD}(\mathrm{mg\,kg^{-1}\cdot day^{-1}}) = \frac{\mathrm{C_p \times\ AIR\ \times\ FE\ \times\ LED\ \times\ UCF}}{\mathrm{BW\ \times\ AT}} \tag{5}$$

where, C_p represents BaP_{eq} concentration of individual PAHs (in ng m^{-3}); AIR is the air inhalation rate: 20 m^3 day^{-1} for adults and 10 m^3 day^{-1} for children[65]; FE indicates frequency of exposure in days: 365 days for both adults and children[32]; LED is the lifetime exposure duration: based on US EPA (USEPA, 2011) guidelines, 24 years for adults to represent typical long-term exposure, and 6 years for children to capture early-life exposure, which is critical because children are more vulnerable to the effects of carcinogens are considered in this study. AT is the average exposure time to carcinogens in days: for both adults and children, the US EPA assumes that health risks from carcinogens are cumulative over a lifetime, and thus considers a lifetime averaging period of 70 years, equivalent to 70 × 365 days[66]; UCF refers to unit conversion factor (from ng to mg); BW represents body weight: 60 kg for adults and 18 years for children (ICMR 2010); CSF (per m kg^{-1} day^{-1}) for all PAHs was considered using the CSF of BaP, and it was taken as 3.1[64].

Emission factor (EF) estimation

EF of PAHs from vehicles passing through the study roadway tunnel during a time interval was calculated using the distance-based equation[67,68] as shown in Eq. (6).

$$\mathrm{EF_{PAH,veh}} = \frac{\left(\mathrm{C_{PAH,exit}} - \mathrm{C_{PAH,entry}}\right)\mathrm{x\ U\ x\ T\ x\ A}}{\mathrm{V\ x\ L}} \tag{6}$$

where $EF_{PAH,veh}$ (mg veh^{-1} km^{-1}) is the average fleet emission factor of PAH; $C_{PAH,exit}$ (μg m^{-3}) represents the concentration of PAH compounds measured 100 m inside the tunnel near the exit, while $C_{PAH,entry}$ (μg m^{-3}) corresponds to the concentration measured 50 m inside the tunnel near the entrance; U (m s^{-1}) is the wind speed parallel to the tunnel sensed by the 3-D sonic anemometer; A (m^2) is the tunnel cross-sectional area, which is 157 m^2 in this study; V is the total number vehicles that travelled through the tunnel during the time interval T (s); and L is the length of the tunnel between the two monitoring stations (at entry and exit) (L is 879 m in South-Bore and 767 m in North-Bore).

Data availability

Data is provided in the supplementary information files.

Code availability

The codes that support the findings of this study are widely used in the community and can be obtained from the first author (sohana.d@iitb.ac.in) upon request.

Received: 27 November 2024; Accepted: 14 February 2025;
Published online: 07 April 2025

References

1. Nagpure, A. S., Gurjar, B. R., Kumar, V. & Kumar, P. Estimation of exhaust and non-exhaust gaseous, particulate matter and air toxics emissions from on-road vehicles in Delhi. *Atmos. Environ.* **127**, 118–124 (2016).
2. Guttikunda, S. & Ka, N. Evolution of India's $PM_{2.5}$ pollution between 1998 and 2020 using global reanalysis fields coupled with satellite observations and fuel consumption patterns. *Environ. Sci.: Atmos.* **2**, 1502–1515 (2022).
3. Lin, H. et al. Particle size and chemical constituents of ambient particulate pollution associated with cardiovascular mortality in Guangzhou, China. *Environ. Pollut.* **208**, 758–766 (2016).
4. Lelieveld, J. et al. Air pollution deaths attributable to fossil fuels: observational and modelling study. *BMJ* **383**, e077784 (2023).
5. Ancelet, T., Davy, P. K., Trompetter, W. J., Markwitz, A. & Weatherburn, D. C. Carbonaceous aerosols in an urban tunnel. *Atmos. Environ.* **45**, 4463–4469 (2011).
6. Mukherjee, S., Dutta, M., Ghosh, A. & Chatterjee, A. A year-long study on PM2.5 and its carbonaceous components over eastern Himalaya in India: contributions of local and transported fossil fuel and biomass burning during premonsoon. *Environ. Res.* **212**, 113546 (2022).
7. Bhardwaj, A., Haswani, D., Yadav, K. & Sunder Raman, R. PM2.5 carbonaceous components and mineral dust at a COALESCE network site—Bhopal, India: estimating site-specific optical characteristics. *Sci. Total Environ.* **880**, 163277 (2023).
8. Yadav, K., Bhardwaj, A. & Sunder Raman, R. Chemical characterization, source identification and potential health effects of PM2.5-bound non-polar organic compounds over a COALESCE network site—Bhopal, India. *Sci. Total Environ.* **920**, 170957 (2024).
9. Rengarajan, T. et al. Exposure to polycyclic aromatic hydrocarbons with special focus on cancer. *Asian Pac. J. Tropical Biomed.* **5**, 182–189 (2015).
10. Mallah, M. A. et al. Polycyclic aromatic hydrocarbon and its effects on human health: an overview. *Chemosphere* **296**, 133948 (2022).
11. Balmer, J. E., Hung, H., Yu, Y., Letcher, R. J. & Muir, D. C. G. Sources and environmental fate of pyrogenic polycyclic aromatic hydrocarbons (PAHs) in the Arctic. *Emerg. Contam.* **5**, 128–142 (2019).
12. Cochran, R. E. et al. Determination of polycyclic aromatic hydrocarbons and their oxy-, nitro-, and hydroxy-oxidation products. *Analytica Chim. Acta* **740**, 93–103 (2012).
13. Fang, X. et al. Characteristics, emissions and source identifications of particle polycyclic aromatic hydrocarbons from traffic emissions using tunnel measurement. *Transp. Res. D: Transp. Environ.* **67**, 674–684 (2019).
14. Rajeev, P., Singh, A. K., Singh, G. K., Vaishya, R. C. & Gupta, T. Chemical characterization, source identification and health risk assessment of polycyclic aromatic hydrocarbons in ambient particulate matter over central Indo-Gangetic Plain. *Urban Clim.* **35**, 100755 (2021).
15. Zhong, M. & Jang, M. Dynamic light absorption of biomass-burning organic carbon photochemically aged under natural sunlight. *Atmos. Chem. Phys.* **14**, 1517–1525 (2014).
16. Samburova, V. et al. Polycyclic aromatic hydrocarbons in biomass-burning emissions and their contribution to light absorption and aerosol toxicity. *Sci. Total Environ.* **568**, 391–401 (2016).
17. Cheng, Y. et al. Brown and black carbon in Beijing aerosol: Implications for the effects of brown coating on light absorption by black carbon. *Sci. Total Environ.* **599–600**, 1047–1055 (2017).
18. Sun, H., Biedermann, L. & Bond, T. C. Color of brown carbon: A model for ultraviolet and visible light absorption by organic carbon aerosol. *Geophys. Res. Lett.* **34**, 2007GL029797 (2007).
19. Huang, R.-J. et al. Brown Carbon Aerosol in Urban Xi'an, Northwest China: the composition and light absorption properties. *Environ. Sci. Technol.* **52**, 6825–6833 (2018).
20. Samburova, V., Zenobi, R. & Kalberer, M. Characterization of high molecular weight compounds in urban atmospheric particles. *Atmos. Chem. Phys*. **5**, 2163(2005).
21. Nguyen, Q. T. et al. Characterization of humic-like substances in Arctic aerosols. *JGR Atmos.* **119**, 5011–5027 (2014).
22. Yuan, W. et al. Concentrations, optical properties and sources of humic-like substances (HULIS) in fine particulate matter in Xi'an, Northwest China. *Sci. Total Environ.* **789**, 147902 (2021).

23. Izhar, S., Gupta, T., Qadri, A. M. & Panday, A. K. Wintertime chemical characteristics of aerosol and their role in light extinction during clear and polluted days in rural Indo Gangetic plain. *Environ. Pollut.* **282**, 117034 (2021).
24. Choudhary, V., Rajput, P. & Gupta, T. Absorption properties and forcing efficiency of light-absorbing water-soluble organic aerosols: seasonal and spatial variability. *Environ. Pollut.* **272**, 115932 (2021).
25. Rajeev, P., Choudhary, V., Chakraborty, A., Singh, G. K. & Gupta, T. Light absorption potential of water-soluble organic aerosols in the two polluted urban locations in the central Indo-Gangetic Plain. *Environ. Pollut.* **314**, 120228 (2022).
26. Alves, C. A. et al. Physical and chemical properties of non-exhaust particles generated from wear between pavements and tyres. *Atmos. Environ.* **224**, 117252 (2020).
27. Fussell, J. C. et al. A review of road traffic-derived non-exhaust particles: emissions, physicochemical characteristics, health risks, and mitigation measures. *Environ. Sci. Technol.* **56**, 6813–6835 (2022).
28. Cheruiyot, N. K. et al. An overview: polycyclic aromatic hydrocarbon emissions from the stationary and mobile sources and in the ambient air. *Aerosol Air Qual. Res.* **15**, 2730–2762 (2015).
29. Keyte, I. J., Albinet, A. & Harrison, R. M. On-road traffic emissions of polycyclic aromatic hydrocarbons and their oxy- and nitro-derivative compounds measured in road tunnel environments. *Sci. Total Environ.* **566–567**, 1131–1142 (2016).
30. Agarwal, A. K., Gupta, T., Bothra, P. & Shukla, P. C. Emission profiling of diesel and gasoline cars at a city traffic junction. *Particuology* **18**, 186–193 (2015).
31. Suman, S., Sinha, A. & Tarafdar, A. Polycyclic aromatic hydrocarbons (PAHs) concentration levels, pattern, source identification and soil toxicity assessment in urban traffic soil of Dhanbad, India. *Sci. Total Environ.* **545–546**, 353–360 (2016).
32. Gope, M., Masto, R. E., George, J. & Balachandran, S. Exposure and cancer risk assessment of polycyclic aromatic hydrocarbons (PAHs) in the street dust of Asansol city, India. *Sustain. Cities Soc.* **38**, 616–626 (2018).
33. Sonwani, S., Saxena, P. & Khillare, P. S. Profile of atmospheric particulate PAHs near busy roadway in tropical megacity, India. *Inhalation Toxicol.* **34**, 39–50 (2022).
34. Debbarma, S., Raparthi, N., Venkataraman, C. & Phuleria, H. C. Impact of real-world traffic and super-emitters on vehicular emissions under inter-city driving conditions in Maharashtra, India. *Atmos. Pollut. Res.* **15**, 102058 (2024).
35. Zhao, T. et al. PM2.5-bound polycyclic aromatic hydrocarbons (PAHs) and their derivatives (nitrated-PAHs and oxygenated-PAHs) in a road tunnel located in Qingdao, China: characteristics, sources and emission factors. *Sci. Total Environ.* **720**, 137521 (2020).
36. Liu, J., Deng, S., Tong, H., Yang, Y. & Tuheti, A. Emission profiles, source identifications, and health risk of polycyclic aromatic hydrocarbons (PAHs) in a road tunnel located in Xi'an, China. *Environ. Sci. Pollut. Res.* **30**, 85125–85138 (2023).
37. Wang, B. et al. Characteristics of particle emissions from light duty diesel vehicle fueled with ultralow sulphur diesel and biodiesel blend. *Atmos. Pollut. Res.* **12**, 101169 (2021).
38. Rajeev, P., Shukla, P. C., Singh, G. K., Das, D. & Gupta, T. Assessment of entrainment of key PAHs emanating from major combustion sources into the ambient air. *Fuel* **347**, 128430 (2023).
39. Ravindra, K., Sokhi, R. & Vangrieken, R. Atmospheric polycyclic aromatic hydrocarbons: Source attribution, emission factors and regulation. *Atmos. Environ.* **42**, 2895–2921 (2008).
40. Lawrence, S. et al. Source apportionment of traffic emissions of particulate matter using tunnel measurements. *Atmos. Environ.* **77**, 548–557 (2013).
41. Katsoyiannis, A. & Breivik, K. Model-based evaluation of the use of polycyclic aromatic hydrocarbons molecular diagnostic ratios as a source identification tool. *Environ. Pollut.* **184**, 488–494 (2014).
42. Ho, K. F. et al. Emissions of gas- and particle-phase polycyclic aromatic hydrocarbons (PAHs) in the Shing Mun Tunnel, Hong Kong. *Atmos. Environ.* **43**, 6343–6351 (2009).
43. Chen, F., Hu, W. & Zhong, Q. Emissions of particle-phase polycyclic aromatic hydrocarbons (PAHs) in the Fu Gui-shan Tunnel of Nanjing, China. *Atmos. Res.* **124**, 53–60 (2013).
44. Gaga, E. O. et al. Determination of real-world emission factors of trace metals, EC, OC, BTEX, and semivolatile organic compounds (PAHs, PCBs and PCNs) in a rural tunnel in Bilecik, Turkey. *Sci. Total Environ.* **643**, 1285–1296 (2018).
45. Wang, W.-C., Dat, N. D., Chi, K.-H. & Chang, M.-B. Characterization of PM2.5 and Particulate PAHs Emitted from Vehicles via Tunnel Sampling in Different Time Frames. *Aerosol Air Qual. Res.* **21**, 210074 (2021).
46. Debbarma, S., Raparthi, N., Venkataraman, C. & Phuleria, H. C. Characterization and apportionment of carbonaceous aerosol emission factors from light-duty and heavy-duty vehicle fleets in Maharashtra, India. *Environ. Pollut.* **345**, 123479 (2024).
47. Zhu, C. et al. *n* -Alkanes and PAHs in the Southeastern Tibetan Plateau: Characteristics and Correlations With Brown Carbon Light Absorption. *JGR Atmos.* **125**, e2020JD032666 (2020).
48. Saleh, R. From measurements to models: toward accurate representation of brown carbon in climate calculations. *Curr. Pollut. Rep.* **6**, 90–104 (2020).
49. Cheng, Y. et al. The characteristics of brown carbon aerosol during winter in Beijing. *Atmos. Environ.* **127**, 355–364 (2016).
50. Zhang, X., Lin, Y.-H., Surratt, J. D. & Weber, R. J. Sources, composition and absorption Ångström exponent of light-absorbing organic components in aerosol extracts from the Los Angeles Basin. *Environ. Sci. Technol.* **47**, 3685–3693 (2013).
51. Kim, H., Kim, J. Y., Jin, H. C., Lee, J. Y. & Lee, S. P. Seasonal variations in the light-absorbing properties of water-soluble and insoluble organic aerosols in Seoul, Korea. *Atmos. Environ.* **129**, 234–242 (2016).
52. Navinya, C. et al. Brownness of organics in anthropogenic biomass burning aerosols over South Asia. *Atmos. Chem. Phys.* **24**, 13285–13297 (2024).
53. Yan, J., Wang, X., Gong, P. & Wang, C. Nitrated polycyclic aromatic compounds in the atmospheric environment: a review. *Crit. Rev. Environ. Sci. Technol.* **51**, 1159–1185 (2021).
54. Wu, D. et al. Source analysis and health risk assessment of polycyclic aromatic hydrocarbon (PAHs) in total suspended particulate matter (TSP) from Bengbu, China. *Sci. Rep.* **14**, 5080 (2024).
55. Gaga, E. O. & Arı, A. Gas-particle partitioning and health risk estimation of polycyclic aromatic hydrocarbons (PAHs) at urban, suburban and tunnel atmospheres: Use of measured EC and OC in model calculations. *Atmos. Pollut. Res.* **10**, 1–11 (2019).
56. Alves, C. A. et al. Polycyclic aromatic hydrocarbons (PAHs) and their derivatives (oxygenated-PAHs, nitrated-PAHs and azaarenes) in size-fractionated particles emitted in an urban road tunnel. *Atmos. Res.* **180**, 128–137 (2016).
57. He, L.-Y., Hu, M., Zhang, Y.-H., Huang, X.-F. & Yao, T.-T. Fine Particle Emissions from On-Road Vehicles in the Zhujiang Tunnel, China. *Environ. Sci. Technol.* **42**, 4461–4466 (2008).
58. Jaiprakash & Habib, G. Chemical and optical properties of PM2.5 from on-road operation of light duty vehicles in Delhi city. *Sci. Total Environ.* **586**, 900–916 (2017).
59. Raparthi, N., Debbarma, S. & Phuleria, H. C. Development of real-world emission factors for on-road vehicles from motorway tunnel measurements. *Atmos. Environ. X* **10**, 100113 (2021).
60. Raparthi, N., Debbarma, S. & Phuleria, H. C. Determination of heavy-duty vehicle emission factors from highway tunnel measurements in India: Laboratory vs. real-world study. *Atmos. Pollut. Res.* **13**, 101581 (2022).
61. Han, Y. M. et al. Carbonaceous aerosols in megacity Xi'an, China: Implications of thermal/optical protocols comparison. *Atmos. Environ.* **132**, 58–68 (2016).

62. Chow, J. C. et al. Separation of brown carbon from black carbon for IMPROVE and Chemical Speciation Network PM $_{2.5}$ samples. *J. Air Waste Manag. Assoc.* **68**, 494–510 (2018).
63. Collins, J. F., Brown, J. P., Dawson, S. V. & Marty, M. A. Risk assessment for benzo[a]pyrene. *Regulatory Toxicol. Pharmacol.* **13**, 170–184 (1991).
64. Singh, D. K. & Gupta, T. Effect through inhalation on human health of PM 1 bound polycyclic aromatic hydrocarbons collected from foggy days in northern part of India. *J. Hazard. Mater.* **306**, 257–268 (2016).
65. Soltani, N. et al. Ecological and human health hazards of heavy metals and polycyclic aromatic hydrocarbons (PAHs) in road dust of Isfahan metropolis, Iran. *Sci. Total Environ.* **505**, 712–723 (2015).
66. Ferreira-Baptista, L. & De Miguel, E. Geochemistry and risk assessment of street dust in Luanda, Angola: A tropical urban environment. *Atmos. Environ.* **39**, 4501–4512 (2005).
67. Zhang, Y. et al. Emission factors of fine particles, carbonaceous aerosols and traces gases from road vehicles: Recent tests in an urban tunnel in the Pearl River Delta, China. *Atmos. Environ.* **122**, 876–884 (2015).
68. Huang, R.-J. et al. Concentration, optical characteristics, and emission factors of brown carbon emitted by on-road vehicles. *Sci. Total Environ.* **810**, 151307 (2022).

Acknowledgements

This study was funded by the Department of Science and Technology (DST), Government of India (Grant no. DST/CCP/CoE/140/2018). We are thankful to Maharashtra State Road Development Corporation Ltd. (MSRDC) Pune for giving the necessary permissions to conduct the measurements. We would also like to thank Nagendra Raparthi, Kamlika Gupta, and Delwin Pullokaran for their support during the course of the measurements.

Author contributions

Conceptualization: H.C.P., S.D.; Methodology: H.C.P., S.D.; Formal Analysis: S.D., P.R.; Software and Visualization: S.D.; Data Curation: S.D.; Writing - Original Draft: S.D.; Writing—Review & Editing: H.C.P., T.G., P.R., S.D.; Supervision: H.C.P.

Competing interests

The authors declare no competing interests.

Additional information

Supplementary information The online version contains supplementary material available at https://doi.org/10.1038/s44407-025-00005-w.

Correspondence and requests for materials should be addressed to Harish C. Phuleria.